Smart Structures and Systems, *Vol. 27, No. 2 (2021) 285-303*
DOI: https://doi.org/10.12989/sss.2021.27.2.285

Structural analysis and health monitoring of twentieth-century cultural heritage: the Flaminio Stadium in Rome

Paolo Di Re [a], Egidio Lofrano [b], Jacopo Ciambella [c] and Francesco Romeo*

Department of Structural and Geotechnical Engineering, Sapienza University of Rome, Via Eudossiana 18, Rome 00184, Italy

(*Received August 13, 2020, Revised September 20, 2020, Accepted October 7, 2020*)

Abstract. This work deals with structural analysis and health monitoring (SHM) of a valuable structure of the twentieth-century cultural heritage: the Flaminio Stadium in Rome. The Flaminio is one of the iconic reinforced concrete sport facilities designed and built by Pier Luigi Nervi for the 1960 Olympic Games of Rome. In view of the foreseen SHM activity, the structural analysis of the Flaminio Stadium is firstly reported by presenting either preliminary analyses, aimed at studying the stadium response under different modeling hypotheses, and a three-dimensional Finite Element (FE) model of the entire structure. It turns out that the main grandstand canopy plays a pivotal role in the Flaminio's structural response to seismic excitation; in addition, its state of conservation raises some concern. Therefore, the structural modeling and dynamic characterization of the canopy is deepened in the paper. Its unusual features, such as geometry, material characteristics and dynamic interplay with the hosting main reinforced concrete frames are thoroughly assessed. To validate the FE results, characterized by a high modal density, and investigate the response of the structure, dynamic tests carried out under operating conditions are presented. The output-only collected data are used to calibrate the initial FE model. The predicted static and dynamic responses of the canopy are eventually exploited to guide the design of a tailored monitoring system. The relevant data management is framed in a heritage building information modeling (HBIM) context. This study draws a viable process for a proactive structural conservation strategy of twentieth-century heritage buildings and infrastructures.

Keywords: structural health monitoring; dynamic tests; proactive conservation; reinforced concrete structure; cultural heritage; Pier Luigi Nervi; HBIM

1. Introduction

Structural analysis and health monitoring of the Pier Luigi Nervi's Flaminio Stadium are considered in this work. The temporal proximity of the heritage of the twentieth century, especially the one made of reinforced concrete, such as the Flaminio Stadium, has delayed a shared attention to the conservation issues that it manifests. The awareness of the historical, architectural and cultural values of the 'recent' architectural heritage, combined with the serious and growing problems of structural safety, today fuels a greater sensitivity to this heritage, making it worthy of protection as a tangible evidence of a particular historical moment, rich in discoveries and experiments on new materials. Conservation planning and management requires a coordinated interdisciplinary approach in which the structural domain plays a crucial role. The physical conditions and structural integrity assessment and management are indeed key prerequisites for any practical conservation policy. The structural conservation process consists of condition survey, identification of the causes of damage and decay, choice of remedial measures and control of interventions efficiency. Each step to be possibly conducted in compliance with cultural heritage general principles, namely minimum intervention, compatibility and reversibility. Once examined documentary and physical evidence, structural diagnostics should be undertaken using carefully considered non-invasive methods. According to ICOMOS/ISCARSAH Guidelines (ICOMOS-ISC20C 2017), the Italian Guidelines published on February 9th 2011 (Presidente del Consiglio dei Ministri – Italia, Italian President of the Council of Ministers 2011), and, more recently, fib Model Code 2020 (Matthews *et al*. 2018), preventive and proactive approaches shall be pursued. The natural choice is to rely on structural health monitoring (SHM) applications, i.e., continuous system identification physical or parametric models of the structure using time-dependent response and environmental data. Structural identification and monitoring of large civil structures, such as long-span bridges, high-rise buildings and sport arenas is a challenging task and is attracting more and more interest from the scientific community. In this research field, vibration-based approaches under operational conditions, e.g., Operational Modal Analysis (OMA), are surely dominant, as the application of external loads is practically unrealistic. For instance, Caprioli *et al*. (2009) discussed the vibration measurement network of the "Giuseppe Meazza

*Corresponding author, Associate Professor,
E-mail: francesco.romeo@uniroma1.it
[a] Research Fellow, E-mail: paolo.dire@uniroma1.it
[b] Research Associate, E-mail: egidio.lofrano@uniroma1.it
[c] Assistant Professor,
E-mail: jacopo.ciambella@uniroma1.it

ISSN: 1738-1584 (Print), 1738-1991 (Online)

Stadium" in Milan, one of the biggest in Italy. In OMA, the goal is to extract as much information as possible from the data acquired during the tests, aiming at characterizing the modal structural behavior. There are several tools and techniques already available in the technical literature for this purpose; we may cite Zhang *et al*. (2010) as one of the successful techniques dedicated to civil engineering structures. When non-proportionality of damping is dominant, see Gattulli *et al*. (2019), specific mechanical interpretations of dissipative properties are needed. In a recent study, Diord *et al*. (2017) showed the influence of different analysis techniques and the dispersion due to long time monitoring for the "Braga Stadium" suspension roof (Braga, Portugal). Even when many sensors and data are exploitable, a structural modelling of the structure is crucial for both identification and monitoring purposes. A paramount example, the Pier Luigi Nervi's Turin Exhibition Centre, is discussed in Lenticchia *et al*. (2017, 2018).

The Flaminio Stadium is in Rome, along the Via Flaminia, close to the city center. The owner of the building is "Roma Capitale", i.e., the Municipality of Rome. The construction is one of the outstanding reinforced concrete sport facilities designed and built by Pier Luigi Nervi for the 1960 XVII Olympic Games. More specifically, it was designed in collaboration with his son Antonio and built by the Nervi & Bartoli construction firm between 1957 and 1959. The stadium was built on the footprint of the National Stadium designed by Marcello Piacentini, demolished in 1957 (Rossi 2013). Listed since September 2018, the Flaminio represents an iconic example of Nervi's structural architecture in which, while adhering to the stadium design principles stated by Nervi himself since 1932 (Olmo and Chiorino 2010, Romeo 2013, Antonucci *et al*. 2014), numerous original and innovative solutions are adopted.

The primary use of the Flaminio Stadium was to host soccer games, but it has been also widely used over the years for other sport disciplines, as music and cultural events. It is decommissioned since 2011 and is now in a despicable neglected state (Tiberi *et al*. 2017). In 2017, the Department of Structural and Geotechnical Engineering of Sapienza University of Rome received from the Getty Foundation (through its "Keeping it Modern" program) a grant for developing the Flaminio conservation plan. In this context, the structural investigations have addressed the safety assessment of the building, mainly focused on its seismic vulnerability.

In the first part of the paper, the main findings concerning with the latter activities are presented. After preliminary analyses aimed at studying the stadium response under different modeling hypotheses, a three-dimensional (3D) Finite Element (FE) model of the entire structure is developed for static and dynamic simulations. The FE model geometric accuracy is consistently derived from the data acquired during a laser-scanner massive survey. The Flaminio canopy, with its overall span of about 27 meters covering 22 main frames, has many peculiarities and its modelling is treated with attention. The canopy is conceived as a bidimensional structure based on the elementary static scheme of a cantilever with backspan. The cast in place backspan is made of extrados beams cooperating with a continuous lower slab, whereas the lighter cantilever is a corrugated roof resulting from a series of adjacent precast ferrocement V-shaped beams. Once assembled, their V-section produce an elegant pleated surface. The two faces of each element delimited above and below by cast in place ribs, are hyperbolic paraboloid surfaces.

The Conservation Plan studies have shown that the west grandstand roof backspan cast-in-place slab (thickness varying from 8 to 15 cm) is affected by widespread damage. The latter is primarily due to prolonged water stagnation caused by the rainwater drain system alteration due to tampering, improper interventions and the presence of shrub weeds. So, the slab is unavoidably affected by carbonation phenomena reaching 20 mm from the downside. Moreover, the current degradation state seems to be amplified by the bad outcome of previous patch repair interventions. In addition, despite its lightness, the canopy plays a key role in the Flaminio seismic behavior due to its position at the top of the west grandstand frames. These aspects urged the Rome Municipality to plan a SHM system devoted to track the evolution of the canopy structural behavior and guide compatible retrofitting interventions.

Towards this goal, thanks to the support of the Department for Sports and Youth Policies of Rome Municipality, an initial experimental dynamic testing campaign has been recently carried out. The experimental results are used to calibrate the material properties adopted in the FE model. Moreover, it is shown how the interpretation of the canopy peculiar dynamics can be used to design a structural health monitoring (SHM) system enabling the assessment of the structural health, the control of the structural degradation, the planning of maintenance works and the evaluation of the increased structural performance achieved by compatible retrofitting interventions. Apart from the numerical and *in-situ* characterization of an iconic structure of the twentieth-century cultural heritage, the paper delineates a SHM strategy concerning with dynamic response rather different from the more usual frame-like and beam-like behavior of common buildings and bridges, respectively. The management of the whole process in a heritage building information modeling (HBIM) framework is eventually discussed.

2. Description of the structure

This section introduces the Flaminio Stadium main structural features. After a brief overview of the overall organization of the structural elements, a subsection focuses explicitly on the grandstand roof and explains its main peculiarities. The material properties are then reported in the closing subsection.

2.1 The stadium

The Stadium designed by Pier Luigi Nervi and his son stands on the same site of a former facility known as the "Torino Stadium", demolished for structural deficiencies.

These was previously called "Stadium of the National Fascist Party" and was the result of refurbishment, designed by M. Piacentini and A. Guazzaroni (1927), of the original structure built in 1911 by M. Piacentini and V. Pardo.

The Flaminio Stadium was originally designed to host soccer matches, with an original seating capacity of 50000 spectators, reduced over time to 20000, due to new safety regulations. It is 181 m × 131 m large, for a total area of 21600 m^2, see Fig. 1, and contains, in addition to the playing field and grandstand seating, four gymnasiums, originally used for gymnastics, boxing, fencing, weightlifting and wrestling, a pool and various services areas, such as coffe bars, changing rooms and first aid stations.

Three typical cast in place reinforced concrete frame shapes have been used by Nervi in the design of the stadium grandstand, see Fig. 2. As shown in Fig. 3(a), the 92 frames are exposed and give the Stadium its peculiar external shape. The distance among the frames is 5.7 m and the mutual transverse connection is realized by grandstand and secondary beams.

Fig. 1 Aerial view of the Flaminio Stadium (ICCD archive)

Grandstand beams were built using two prefabricated reinforced concrete elements, based on the original system invented and patented by Nervi for the Flaminio. This system consists of a U-shaped load bearing element, working also as rainwater collection system, and a second element, placed on top of the first, forming the steps and seats.

The foundation system consists of deep foundations (pile foundation system). Two types of "Franki" cast on site piles are used, with diameter of 335 mm and 500 mm. For each frame, a reinforced concrete beam connects the pile caps at the base of the two columns. These grade beams have rectangular 30 cm × 30 cm cross-section and hold the horizontal tensile force arising at the base of the frames.

The west grandstand is covered by the canopy, Fig. 3(b), whose design and construction is discussed in detail in the following subsection.

2.2 The grandstand canopy

The main grandstand canopy is certainly one of the most interesting structural elements of the Flaminio Stadium. The driving design criteria for a stadium grandstand canopy were discussed by Nervi as early as 1933, in a paper published in Casabella (Nervi 1933), where the author, besides mentioning the benefits provided by the adoption of different materials and different static schemes, focuses on reinforced concrete solutions. The main design issue pointed out by Nervi is related to the thermal stresses induced by the temperature variations between the top and bottom side of the canopy. Therefore, the canopy load bearing elements shall be designed entirely on one side of the roof. This is the case of the Berta stadium, where the structural system is placed below the top 12 cm thick slab,

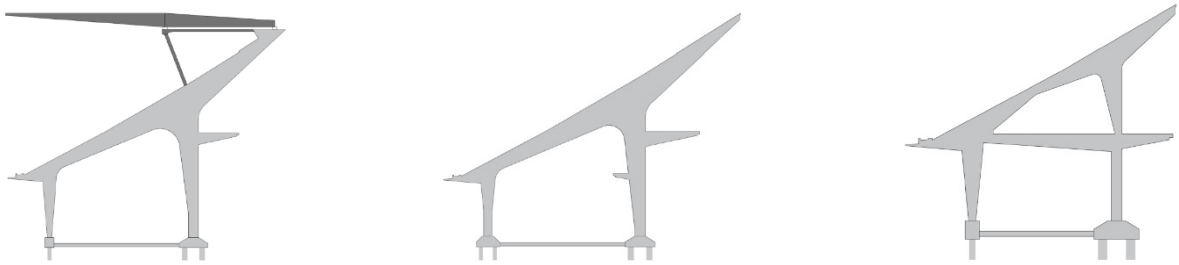

(a) Covered west grandstand (b) Un-covered east grandstand (c) Curves

Fig. 2 Frames used in the Flaminio Stadium

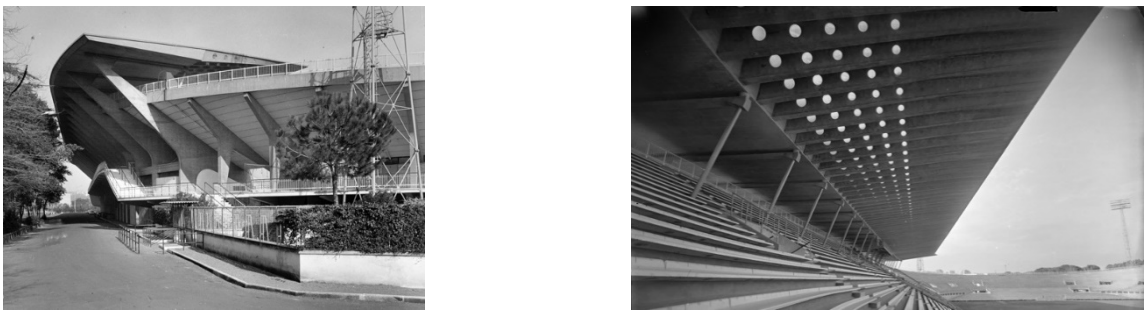

(a) Frames (ICCD archive) (b) Covered west grandstand (ICCD archive)

Fig. 3 Picture of the stadium

the continuity of which is interrupted by expansion joints located every three spans.

Irrespective of the chosen static scheme, an important aspect highlighted by Nervi is that the centroid of the canopy structural system should fall within the two supports of the frame to guarantee compression on all bottom columns and ease their foundations.

In previous stadiums designed by Nervi, grandstand's roof was conceived as a reinforced concrete slab resting on equally spaced structural frames. Given their load bearing role, the frame elements, especially those belonging to the rear subsystem sustaining the overhanging cantilever arms, were unavoidably relatively voluminous, even if with a neat geometry. Hence, by reinterpreting and renewing both static scheme and materials, yet sticking to the basic principles and functional requirements, an improved structural composition is conceived for the Flaminio (Adriaenssens and Billington 2013).

The roof itself is designed as a bidimensional structure based on the elementary static scheme of a cantilever with backspan. In particular, the cast in place backspan is made of a series of extrados beams, connected by a continuous lower slab, whereas the lighter cantilever is a corrugated roof resulting from a series of adjacent ferrocement V-shaped beams. Ferrocement is a type of thin wall reinforced concrete commonly constructed of hydraulic cement mortar reinforced with closely spaced layers of continuous and relatively small size wire mesh; the mesh may be made of metallic or other suitable materials. The two subsystems adopted for backspan and cantilever are connected by a transverse (i.e., parallel to the long side of the stadium) cast in place beam with trapezoidal cross-section, called "M" beam. A further transverse connecting beam with rectangular cross-section is located close to the roof external edge, called "E" beam. Both the backspan and the cantilever are characterized by variable cross-sections. The ferrocement element shape, guided by the bending moment diagram, ranges from a V-shape geometry at the fixed end to a thin, straight rectangular geometry at the free end. The cast in place extrados beams have a pseudo-rectangular cross-section, whose height increases towards the middle transverse beam.

The covered grandstand rest on 22 main frames (no. 82 to 92 and no. 01 to 11) and each of them supports a roof portion made of four V-beams and the corresponding four rear extrados beams. The roof is simply supported over the grandstand at two points: at the exterior, on top of the reinforced concrete frames, in correspondence of the "E" beam, and halfway along the overall span, in correspondence of the "M" beam, where it is supported on inclined steel tubes, filled with reinforced concrete.

Having introduced the general features of the grandstand roof, in view of the in-depth structural analysis that is carried out in the following, the main geometric and structural details, as documented by the archive drawings and documents (CSAC Archive), are reported next. They

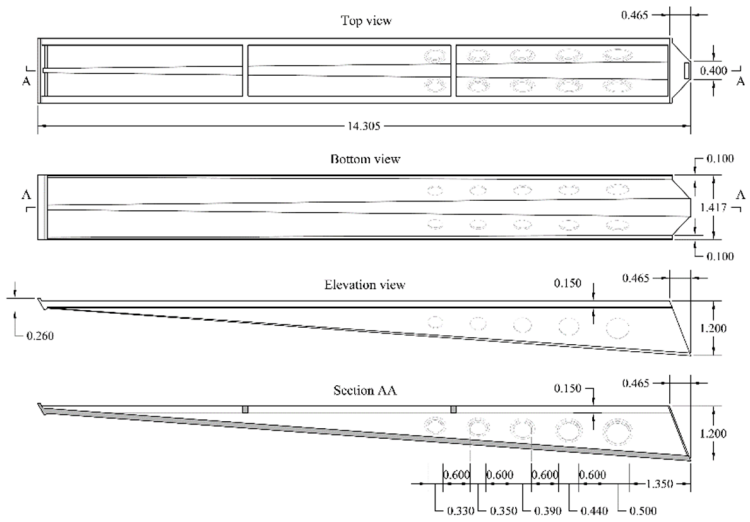

(a) Geometric details (dimensions are in meters)

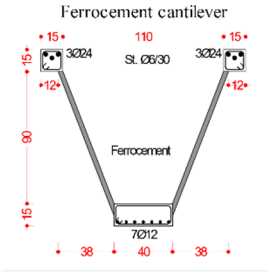

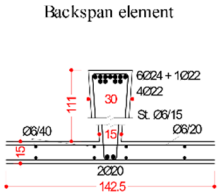

(b) Cross-sections of the canopy elements (dimensions are in centimeters)

(c) Photograph of an experimental test (MAXXI archive)

Fig. 4 Ferrocement wave elements

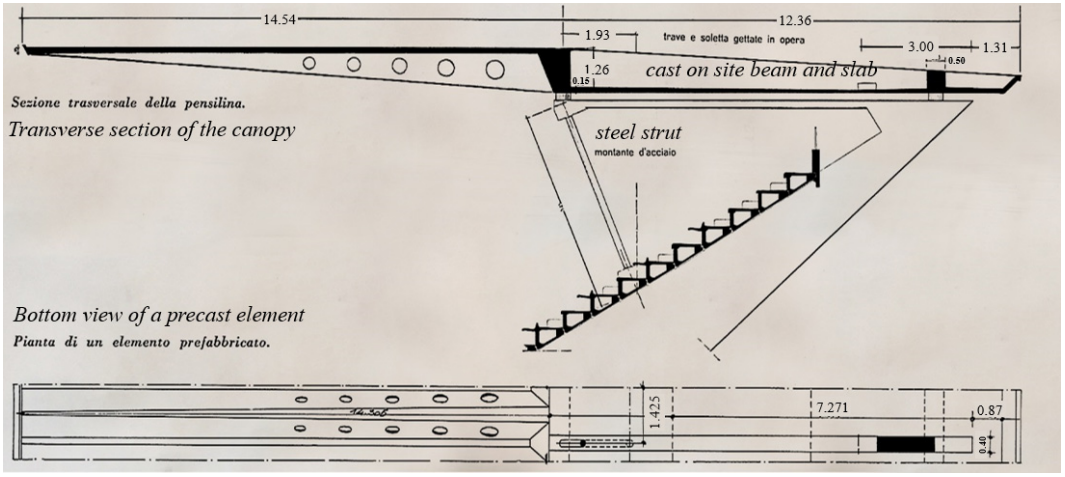

Fig. 5 Canopy structural configuration: section between two consecutive waves of the final version (dimensions are in meters); adapted from the paper by Nervi, P. L. and Nervi, A. (1960)

refer to the final configuration, resulting from updating a rather different initial design proposal. As far as the 14.60 m span cantilever, the ferrocement wave elements (Fig. 4(a)) variable height ranges from 1.20 m to 0.26 cm. The backspan cast in place part consists of a series of extrados beams with trapezoidal cross-section (15 cm width at the bottom and 30 cm at the top) with a lower continuous slab, with variable thickness from 15 cm to 8 cm. Fig. 4(b) shows the cross-sections of the V-shaped cantilever and backspan extrados beam, in correspondence of the "M" beam, where the elements have maximum height. The width of the V-shaped element and the interaxle distance of the backspan extrados beams is 1.425 m (four per each main supporting frame). The relative position of the cantilevered elements and the backspan beams is such that the rectangular cross-section of the latter can host the upper reinforcement bars (3 ø 24) left protruding from the wave elements cast in place upper ribs. This version of the roof structural system was tested on site by using the mock-up shown in Fig. 4(c). This was conceived to test the overhanging ferrocement cantilevers and their connection with the rear cast in place extrados beams. In fact, a counterbalancing scheme was realized, made of two opposite ferrocement cantilevers joined through cast in place beams.

The ferrocement V-beams are composed of 3 layers of steel, one lower and two higher, weighting 0.8 kg/m^2. The overall weight of one wave element is 5.5 tons and two cranes, with a maximum lifting load of 3 tons each, were needed to lift one element. Additional diffused ø 6 rebars were adopted to stiffen the V-shaped element. The 12 cm × 15 cm stiffening transverse ribs positioned at 1/3 and 2/3 of the length, were used to lift the elements with the cranes and position them on the temporary scaffolding. Further transverse stiffening is provided by the slanted fixed end diaphragm. The five circular openings with varying diameter placed on each side were devised to lighten the elements, while allowing passage of light.

In 1958 the configuration of the canopy structural system was finalized by introducing a tie beam connecting the two roof supports, thereby explicitly differentiating the structural roles played by each component (Fig. 5). By doing so, the enlarged top part of the frame is exploited as anchoring point for the tie beam, which has width equal to that of the main frame and is left visible at 20 cm below the roof slab.

A clear distinction is made between the roof and its underlying support structure. This distinction is further emphasized by the two reinforced concrete short cylinders, having 40 cm diameter and 20 cm height (reinforced by 6 ø 20 rebars), located on top of the inclined steel tube and of the frame. In essence, the support structure resting on the frame is a strut and tie truss scheme, for which an apparently counterintuitive choice of materials is employed: the strut is a steel tube (diameter equal to 20 cm, thickness equal to 1 cm), filled with reinforced concrete (6 ø 24 rebars, ø 6/15 cm helicoidal stirrup), Figs. 6(a) and (b), while the tie is a reinforced concrete 20 cm × 40 cm beam (reinforced by 6 ø 20 rebars and ø 6/20 cm stirrups). In truth, the adoption of steel elements for the struts was mainly driven by the intention of not limiting the sight of the spectators. The cross-section of the rear transverse "E" beam is 50 cm × 60 cm, while the middle "M" beam is 126 cm × 60 cm (average width). Both are multiple spans continuous beams resting on supports spaced 5.70 m apart, according to the underlying frame arrangement. Rectangular holes at the bottom of the "M" beam allow the passage of the rainwater collected by the V-beams towards the drainage pipe located in the backspan lower slab.

2.3 Mechanical properties of structural materials

Concrete was used in the construction of the Stadium in several ways and original forms: the *in-situ* casting of the large structural frames, the prefabricated elements of the grandstands, the undulating ferrocement panels of the canopy cast on site in specially designed formwork. Stiffness and strength of the materials and the other mechanical parameters required for the structural analysis and safety checks are determined based on *in-situ* investigations performed over the time (Ragusa *et al*. 1959, G.I.A. L.T.D. 2007, Risorse per Roma S.P.A. 2013, Franceschetti 2015, Romeo and Di Re 2019).

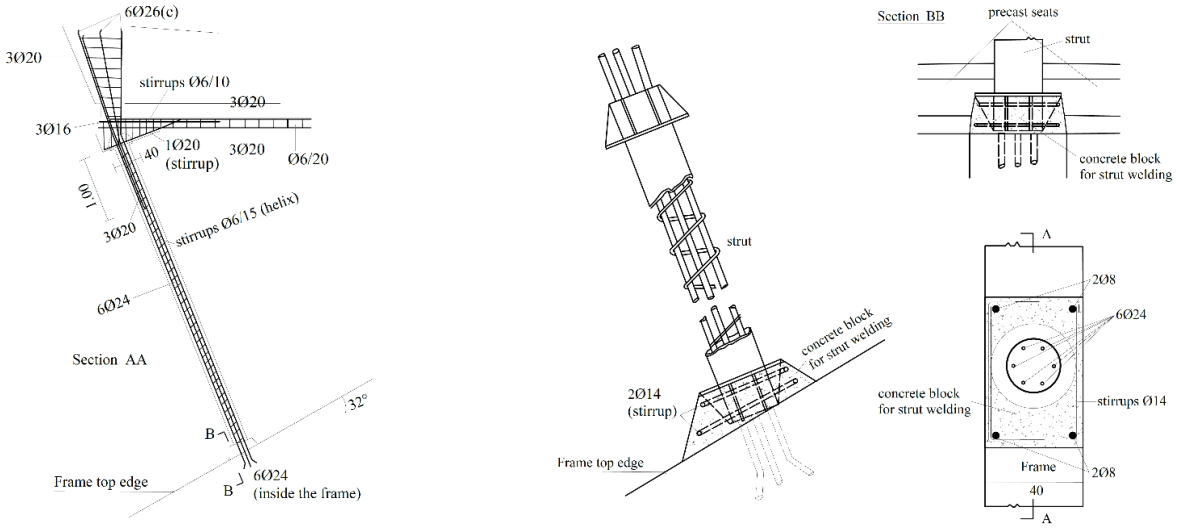

(a) Strut rebars (b) Strut anchorage detail

Fig. 6 Final canopy structural configuration (adapted from the original drawings by Pier Luigi Nervi)

Table 1 Average mechanical properties of structural materials

Material/Properties		Values	Source
Concrete for super-structure*	Young's modulus	30571 MPa	NTC 2018
	Poisson's coefficient	0.2	NTC 2018
	Cylinder compressive strength	29.9 MPa	Tests
	Cylinder tensile strength	2.4 MPa	NTC 2018
	Density	24 kN/m^3	Tests
Concrete for foundations	Young's modulus	33667 MPa	NTC 2018
	Poisson's coefficient	0.2	NTC 2018
	Cylinder compressive strength	41.3 MPa	Tests
	Cylinder tensile strength	3.1 MPa	NTC 2018
	Density	24 kN/m^3	Tests
Reinforcing steel	Young's modulus	210000 MPa	NTC 2018
	Yield stress	390.7 MPa	Tests
	Ultimate strength	549.0 MPa	Tests
	Ultimate strain	19.85 %	Tests
Steel (for canopy struts)	Young's modulus	210000 MPa	NTC 2018
	Poisson's coefficient	0.3	NTC 2018
	Yield stress	450.0 MPa	NTC 2018
	Ultimate strength	557.0 MPa	Tests
	Density	77 kN/m^3	NTC 2018

*Since no data is available for ferrocement, its properties are here assumed equal to those of the concrete used for the super-structure, except for weight for unit volume, assumed equal to 20 kN/m^3, as specified by Nervi

Considering the data retrieved from the available documentation, the average mechanical properties of concrete and reinforcement steel are determined, see Table 1. For the mechanical parameters not available from the tests, reference is made to the Italian code "NTC 2018" (Consiglio Superiore dei Lavori Pubblici – Italia, Italian Superior Council of Public Works 2018). Since no data is available for ferrocement, its properties are here assumed equal to those of the concrete used for the super-structure, except for the weight for unit volume, which is assumed equal to 20 kN/m^3, as specified by Nervi.

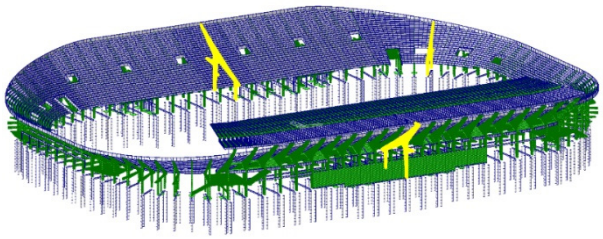

Fig. 7 Complete FE structural model of the stadium

3. Numerical modelling

To study the response of the stadium, a complete 3D FE model involving all the structural elements is defined. Fig. 7 shows a perspective view of the model, created with a commercial FE software (Midas 2018). The main details of the model and the steps performed for its creation are described in the following.

3.1 Modeling of the grandstands and curves

The grandstands and curves of the stadium are modeled by adopting shell and beam FEs. Shell FEs with 3 or 4 nodes are used to represent the non-prismatic geometry of the reinforced concrete main frames, having variable cross-section members and large panel zones at the connection between the vertical columns and oblique beams (see Fig. 8(a)). The shell FE formulation is based on the Mindlin-Reissner plate theory, which includes plate shear deformations, but is properly defined to avoid shear-locking issues (Katili 1993).

Preliminary analyses were conducted on three single frames, to investigate their in-plane behavior under static and dynamic loadings and to explore the possibility of modeling these members through beam equivalent FEs: one for the covered grandstand (no. 01), one for the curves (no. 33) and one for the uncovered grandstand (no. 46). These are highlighted in yellow in Fig. 7. For brevity, a detailed description of these analyses is not reported here, but further data are available in Romeo and Di Re (2019). In this report, it is shown that modeling the frames through beam FEs reduces the computational demand without a significant loss in accuracy. As an example, for frame 01 (central frame of the covered grandstand), the first fifteen in-plane natural vibration modes are determined with both shell and equivalent beam FE models, assuming independent behavior of the frame with respect to the rest of the structure. Corresponding vibration frequencies are compared in Fig. 9, while Fig. 10 shows the modal shape obtained for the first natural mode. As shown by the two figures, the two modeling approaches practically give the same dynamic response for the frame, with a maximum discrepancy in terms of natural frequencies lower than 4%. However, as expected, more accurate results are obtained from the shell model in terms of stress distribution, in particular for the diffusive zones at the intersections between the vertical columns and the oblique beam of the frame, where stress concentrations arise. For instance, Fig. 8(b) plots the distribution of the maximum principal stresses occurring in these zones for the main frame 01 and clearly shows that these are strongly affected by stress concentration phenomena that beam FE models are not able to capture.

Hence, the shell modeling approach is applied to ensure high level of accuracy of the results. Moreover, considering that the stadium is characterized by many different frame geometries, this approach simplifies the modeling operations: a detailed representation through equivalent beam FEs would require a very expensive modeling work for the operator, while the shell model is straightforward from this standpoint. Indeed, starting from the available original graphic drawings and survey data, previously converted into CAD and BIM format, the frames geometries are semi-automatically transformed into shell FE meshes, with a significant time saving for the modeling operations.

Shell FEs are also used to model the structural walls located in the lower part of the covered grandstand, resulted from a structural improvement intervention made in 2007, the concrete-framed glass blocks, located in both grandstands between the frames, and the structural elements of the stairs. All slabs and walkways are modeled as rigid diaphragm elements, except for the spans affected by the structural joints, that is between frames no. 92-1, 11-12, 23-24, 35-36, 46-47, 57-58, 69-70 and 81-82, where explicit

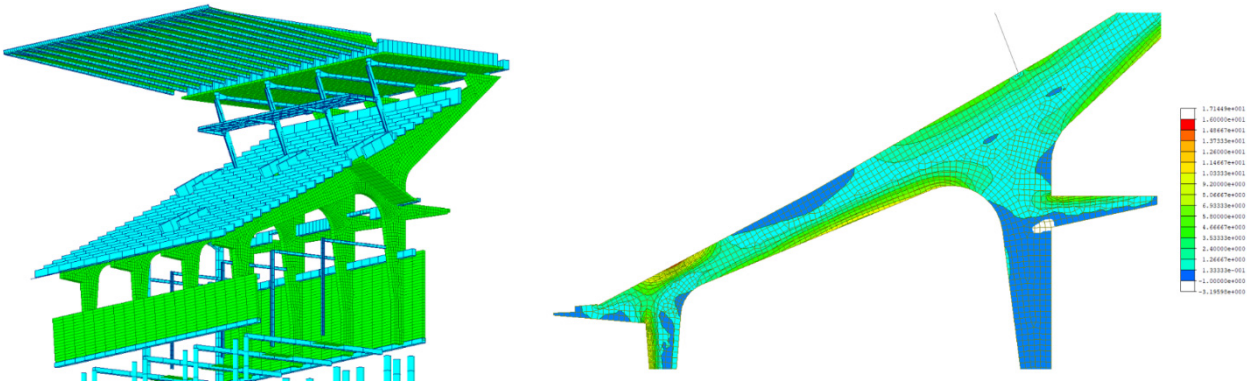

(a) Extruded view for the elements

(b) Maximum principal stresses acting in the main frame no. 01 under static loads (values in MPa)

Fig. 8 Portion of the FE model extracted from the covered tribune

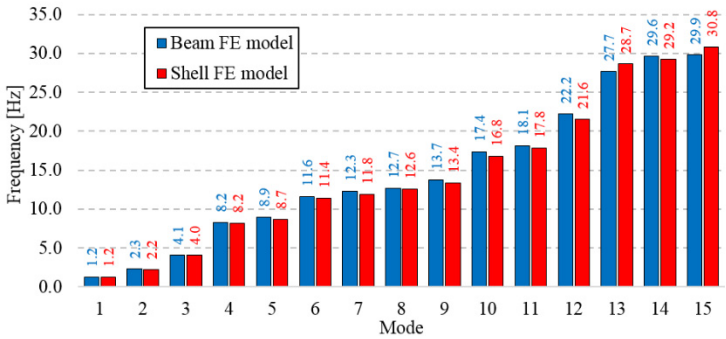

Fig. 9 First 15 in-plane modal frequencies obtained for frame 01 with the beam and shell models

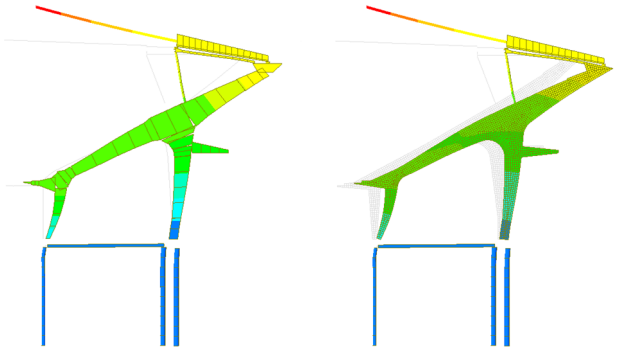

(a) Beam model (b) Shell model

Fig. 10 First in-plane modal shape obtained for frame 01

modeling of these members through shell FEs is adopted. In fact, the survey operations revealed that, although structural joints were realized in these zones between grandstands and between the elements of the canopy (which is divided into two parts), the slabs were created as continuous elements. Hence, to accurately account for the mutual connection of each part of the stadium, the slabs of these zones are modeled through shell FEs.

The remaining members are modeled through beam FEs. These are formulated according to the force-based beam approach (Ciampi and Carlesimo 1986, Spacone *et al*. 1996), which ensures higher performances compared to the classic displacement-based formulation, and considering a consistent definition of the element mass matrix (Bathe 2006, Di Re *et al*. 2019) to includes both translational and rotational inertia terms.

For the grandstand beams, instead of the U-shaped geometry, Nervi considered as resisting cross-section only the area corresponding to the vertical webs. The same assumption is made in the FE model, as shown in Figs. 7 and 8(a). However, to prevent unrealistic transverse deformations of these beams, not allowed in the real structure, rigid trusses are added to connect each FE with the adjacent ones in the direction orthogonal to their axes and parallel to the slope of the bleacher.

All the rectangular beams connecting the main frames (running in the orthogonal direction to the frame planes) and all the elements composing the intermediate frames (located between the main frames) are modeled through beam FEs as well.

Foundation piles are explicitly modeled as cylindrical beam FEs, with springs simulating the stiffness of the soil (Gazetas 1991, Viggiani 1993). Three sets of springs uniformly distributed along the beam axis are assigned, two acting in the horizontal plane, and one working in the vertical direction. In addition, a concentrated spring is applied at the base of each pile. At the top, piles are connected to the bases of the frames through rigid links modeling the plinths. Lastly, the foundation ties are modeled as an additional square beam FEs.

A similar approach is used to model the plinths located under the intermediate columns. These are square shaped with side dimension equal to 1.2, 1.4, 1.5, 1.7, 1.9, 2.0 or 2.45 m. Hence, rigid square horizontal plate elements are used to model these elements, which are rigidly connected to the base of the upright column, whereas distributed springs acting in the three spatial directions are applied to the base of the plate to simulate the soil stiffness.

3.2 Grandstand canopy modeling

To describe the complex geometry of the canopy, a simplified model is created, made of shell and beam FEs, as depicted in Fig. 11. Beam FEs are used to model the canopy support system, with mixed steel-concrete circular cross-sections (for the oblique struts) and square concrete cross-sections (for the horizontal ties). Beam FEs are also used for the steel elements composing the radio reporter platform and for the reinforced concrete “M” and “E” beams. Shell FEs are used to model the intrados slab of the reinforced concrete backspan part of the canopy, whereas equivalent rectangular beam FEs are used to model the vertical variable ribs. For the ferrocement overhang part, shell FEs are used to model the variable V-shaped elements and beam FEs are used to model the ‘core’ beams elements and the transverse connecting beams that run parallel and orthogonal to the V-shaped, respectively. The shell FEs lie in the midplane of the V-shaped element webs and have uniform thickness equal to 3 centimeters. The circular holes located near the “M” beams (Fig. 5) are neglected, while the small overhang slab located at the external edge of the backspan is included in the model as equivalent load and mass.

To verify the accuracy of this simplified model and to validate its relevant performances in representing the structural response of the canopy, a comparative study is

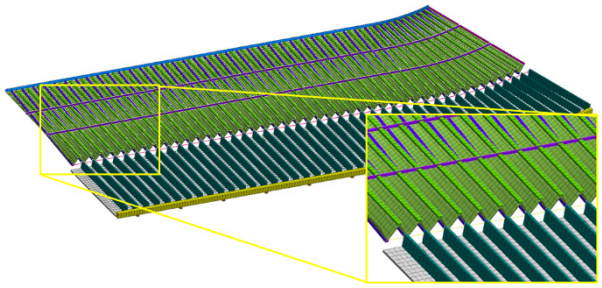

Fig. 11 Simplified (shells plus beams) FE model of the south half of the canopy

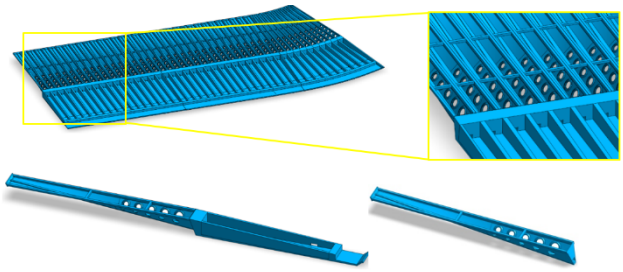

Fig. 12 'Exact' geometry of the south half of the canopy

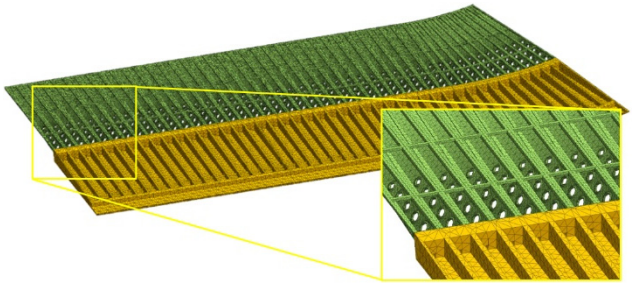

Fig. 13 Accurate (solid) FE model of the south half of the canopy

performed. The canopy, without its support system, is extracted from the rest of the structure and analyzed as a separate body. Because of the symmetry, only the south half of the canopy is considered. It is assumed as simply supported (pinned constraints) at the intrados of the backspan, where the actual reinforced concrete cylindrical supporting elements are located (Fig. 11). Hence, the first 20 natural vibration modes are determined and compared with those resulting from another FE model of the same half of the canopy that adopts solid FEs to accurately reproduce the complex geometry of each structural member.

To create this model, the 'exact' geometry of the half of the canopy is reproduced by using the 3D CAD modeling and rendering software, Rhino (www.rhino3d.com), and then it is imported into the FE software MIDAS FEA NX (Midas 2020), also distributed by the engineering software-house CSPFea (Fig. 12). This geometry is used to create the solid FE mesh in Fig. 13 and perform an accurate structural analysis of the canopy. Higher (quadratic) order 10-nodes tetrahedral elements are used for the FE mesh, based on standard displacement approach (Bathe 2006).

In addition to the concrete and ferrocement self-weight, a uniform distributed permanent load equal to 0.386 kN/m^2 is applied over the entire canopy extrados surface. The total weight of the model, as results from the simplified (shells plus beams) and accurate (solid) model, is equal to 8279 and 7499 kN, respectively, i.e., the simplified model slightly overestimates the canopy mass, with an error of 10.4%. However, both values are in good agreement with that resulting from the analysis of the data reported in Nervi's design reports, equal to 7904 kN.

Fig. 14 compares the values obtained for the modal frequencies from the two models and, as example, Fig. 15 shows the modal shapes associated to modes 1, 3 and 9, respectively. A very good agreement exists between the two solutions. Mode shapes are practically identical, while frequency values show an error lower than 5% for the first eight modes and lower than 14% for the higher modes.

Hence, the adoption of the simplified modeling approach of the canopy is here preferred for the complete complete model of the stadium, as this results almost as accurate as the detailed solid modeling approach, with a significant computational saving. For the studied half of the canopy, indeed, the shells plus beams model in Fig. 11 uses a total of 23239 FEs, whereas the solid model in Fig. 13 requires 459099 FEs.

3.3 Static and seismic loadings

Two kind of static loadings are assigned into the model:

- self-weight of all the structural elements, which is automatically computed and applied by the software, based on geometry and mass density of the elements;
- additional permanent load due to non-structural elements. This loading is assumed equal to 0.7

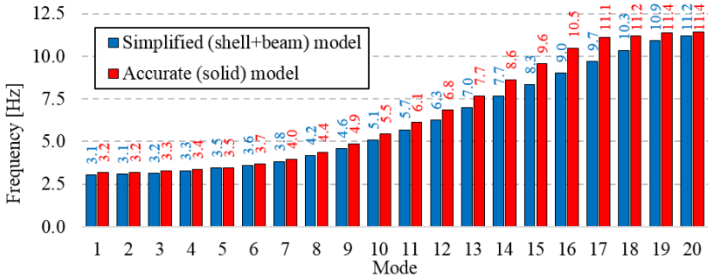

Fig. 14 Comparison of the first 20 modal frequencies obtained for the south half of the canopy with the simplified (shells plus beams) and accurate (solid) FE models

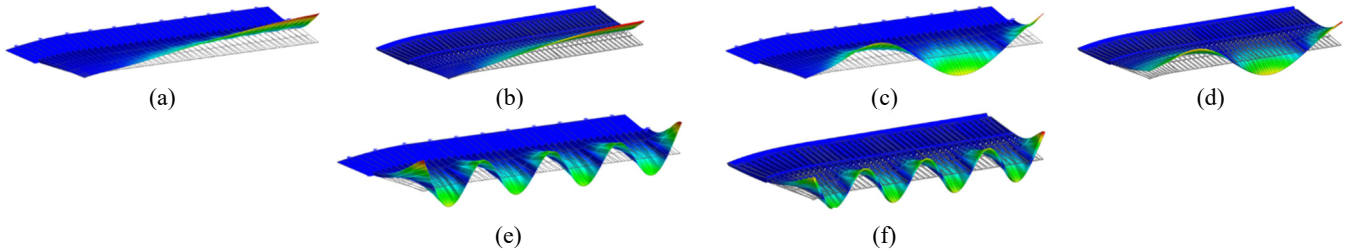

Fig. 15 Comparison of the 1st, 3rd, 9th modal shapes obtained for the south half of the canopy with (a),(c),(e) the simplified (shells plus beams) and (b),(d),(f) the accurate (solid) FE models

kN/m^2 on the grandstands, 1.0 kN/m^2 on the slabs, walkways and stairs, and 0.386 kN/m^2 on the canopy. At the internal tip of the canopy, the weight of the lighting system is also considered, as a force per unit length of 0.2 kN/m.

These loadings are used to define the mass of the structure required in the eigenvalue analysis reported in the following and used as reference calibration solution for the experimental tests described in Section 4. A complete structural analysis is also performed but is not reported here for the sake of brevity, as this is not the focus of the presented study. To this purpose, variable loads, i.e., anthropic, snow, wind, temperature and seismic actions, are also considered. As reference, a uniform anthropic load equal to 5.0 kN/m^2 and 0.5 kN/m^2 is applied over the grandstands and the canopy, respectively, while seismic loads acting in both horizontal plane (x-y) and vertical direction (z) are considered. These are defined according to the Italian construction technical codes (Consiglio Superiore dei Lavori Pubblici – Italia, Italian Superior Council of Public Works 2018), considering the structure as belonging to category C5 and usage class III, working life V_N equal to 100 years, subsoil category C and topographical category T1. Starting from this input, NTC2018 provides the pseudo-acceleration spectra for the limit state analysis of the structure. As an example, the design spectra for Life Safety limit state considers a not-exceeding probability values P_{VR} equal to 10%, a return period T_R equal to 1424 years, a peak ground acceleration a_g equal to 0.137 g, for the horizontal component, and 0.068 g, for the vertical component, a ratio F_0 between the maximum spectral acceleration and a_g equal to 2.694 and a reference period T_C equal to 0.505 s, for the horizontal component, and 0.150 s, for the vertical component. The behavior factor "q" is assumed as the lowest value permitted by the code, i.e., q = 1.5.

A detailed description of the structural analyses is available in Romeo and Di Re (2019). Here, since the Italian code for constructions usually results too conservative for shear safety checks, a detailed modeling of the members under shear action is performed, following the fib Model code (Taerwe and Matthys 2013) and the Simplified Modified Compression Field Theory (Bentz *et al*. 2006).

3.4 Eigenvalue analysis

Modal decomposition of the structure is performed by using the FE model described above. Fig. 16 shows the values of the natural frequencies for the first 50 modes, while Fig. 17 plots, the corresponding participating masses in the three spatial directions, being *x* the horizontal

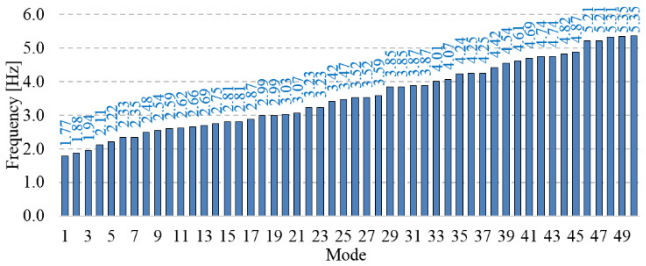

Fig. 16 First 50 natural vibration frequencies of the stadium

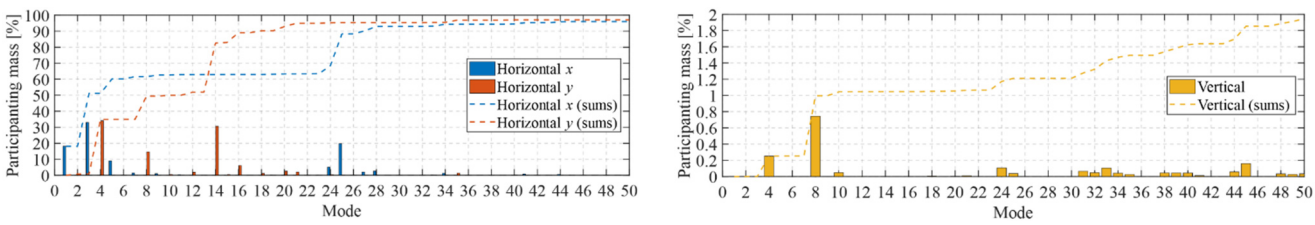

(a) Horizontal modes (b) Vertical modes

Fig. 17 Participating masses for the first 30 natural vibration modes of the structure

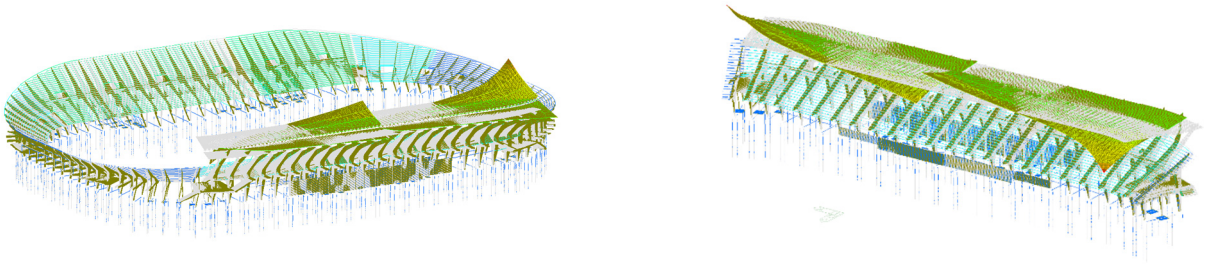

(a) Entire stadium (b) Covered tribune only

Fig. 18 Natural vibration shape of mode 1

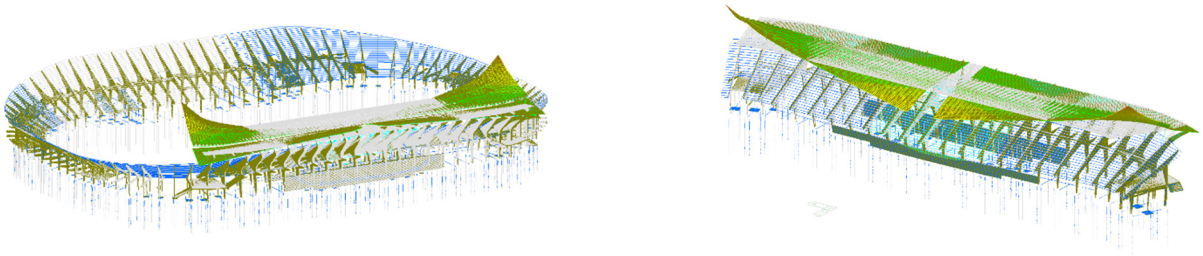

(a) Entire stadium (b) Covered tribune only

Fig. 19 Natural vibration shape of mode 3

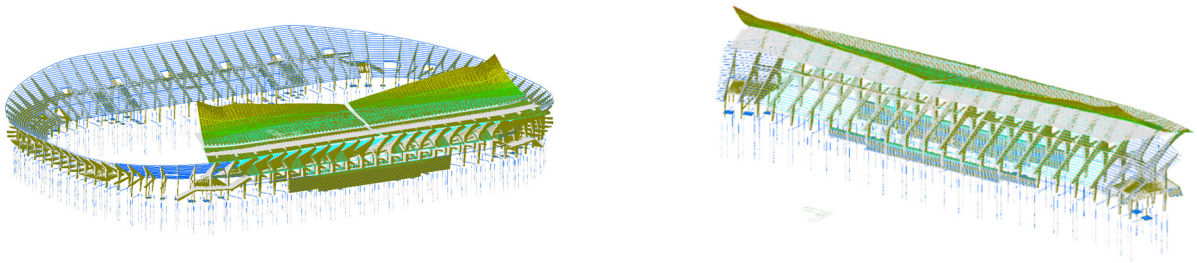

(a) Entire stadium (b) Covered tribune only

Fig. 20 Natural vibration shape of mode 4

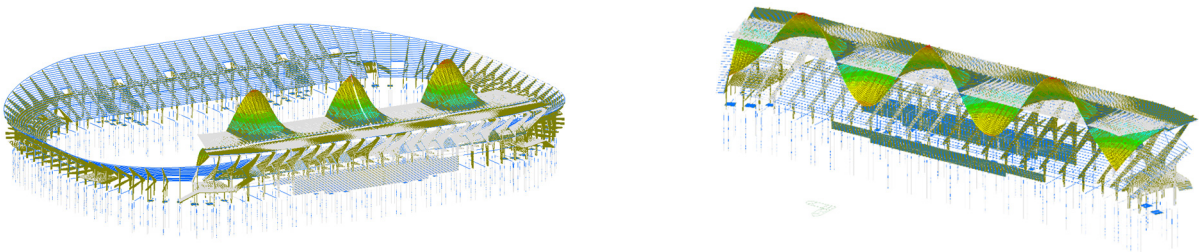

(a) Entire stadium (b) Covered grandstand only

Fig. 21 Natural vibration shape of mode 14

direction parallel to the grandstand, *y* the one orthogonal to the grandstand and z the vertical direction.

Modes 1 and 3 mainly involve mass acceleration in the *x* direction, with mode 3 resulting the prevalent mode in this direction. Their vibration shapes are plotted in Figs. 18 and 19, respectively, considering (a) a view of the entire model and (b) a view of the covered grandstand only. The deformed shape is plotted in colors and is overlapped on the undeformed shaped, which is plotted in gray. To be noted is that the main contribution to the mass excitation in the *x* direction is due to the motion of the grandstands, whose frames deform out of their planes, and to the motion of the canopy. Indeed, significant distortion is observed for the external overhang beams of the frames and for the canopy support struts in the covered grandstand, because of the horizontal translation of the canopy.

Modes 4, 8 and 14 mainly involve mass acceleration in the *y* direction, with mode 4 resulting the prevalent mode in this

direction. Its vibration shape and that of mode 14 are plotted in Figs. 20 and 21, respectively. As shown, mode 4 also excites the largest percentage of mass in the vertical direction, which is mainly due to the vertical motion of the canopy, although this represents a small part of the whole mass of the structure. Similar behavior is observed for mode 8.

A result to be stressed is the high modal density of the structure. In fact, the first 50 frequencies of the model (see Fig. 16) are concentrated in a range of just 3.58 Hz (from 1.77 to 5.35 Hz). This circumstance makes the dynamic structural identification of the stadium truly challenging.

4. Experimental campaign and model calibration

4.1 Dynamic tests

In May 2020, an initial assessment of modal frequencies and shapes was carried out on the stadium canopy. The experimental campaign was intended to both preliminary validate the numerical model (see Section 3), and to evaluate the level of expected environmental vibrations, which is a fundamental information for planning the permanent network of sensors to be deployed on the canopy. During this initial assessment, three different type of sensors were used (see Fig. 22): one autonomous wireless low-cost MEMS accelerometer and two high accuracy sensors (PCB 393A03, Moho Tromino). This allowed to establish a comparison between the low-cost MEMS and the other instruments which serve for validation.

Table 2 provides an overview of the main characteristics of the sensors. The PCB 393A03 are the only wired uniaxial sensors of the three, and the data acquisition was performed through NI board connected to a laptop; these sensors were arranged in a tri-axial configuration for each measurement point. The other accelerometers were wireless, both equipped with on-board ADC, data storage and GPS receiver for time-synchronization between multiple units. The use of wireless sensors for continuous monitoring of structures could provide benefit, such as reduced installation and maintenance costs (Sun *et al*. 2015). However, time synchronization is a key factor to enable the

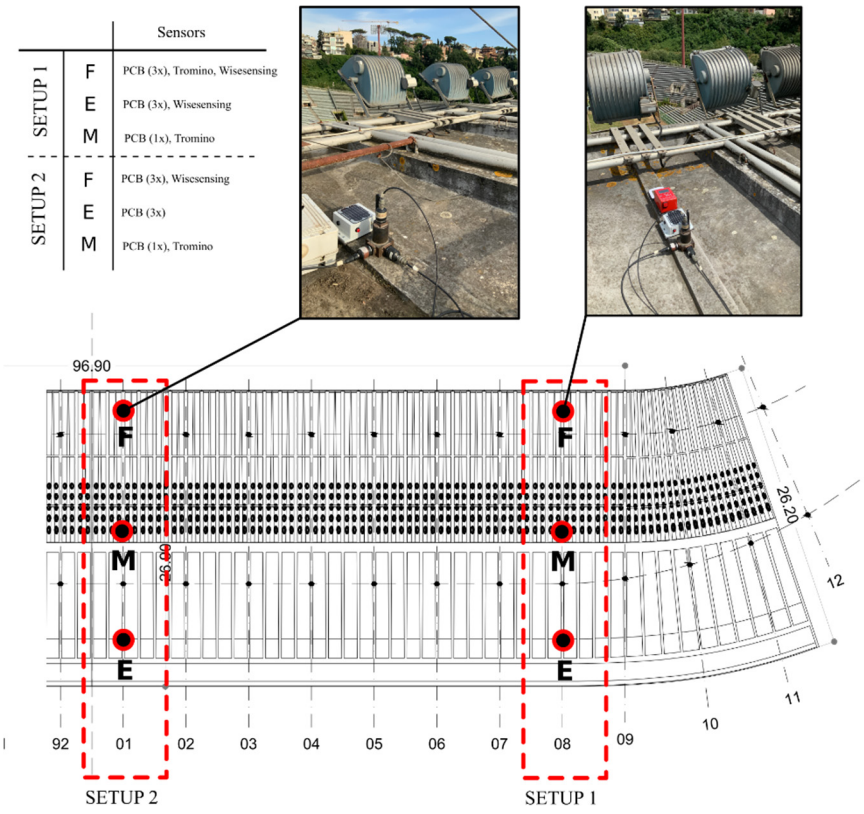

Fig. 22 Experimental tests: accelerometers and setups (dimensions are in meters)

Table 2 Main properties of the accelerometers used for the experimental campaign

Owner	Connections	Channels	Acceleration	Sensitivity	Noise level	Cost
PCB 393A03	Wired	1	± 5 g	± 10 μg	2 μg/$\sqrt{Hz}$	€ 600*
Wisesensing	Wireless	3	± 2 g	± 244 μg	25 μg/$\sqrt{Hz}$	€ 800
Tromino	Wireless	3	± 2 g	± 100 μg	Not available	> € 5000

*The cost of the sensor does not include the cost of the data acquisition system, which can be roughly estimated to be € 1000 per channel

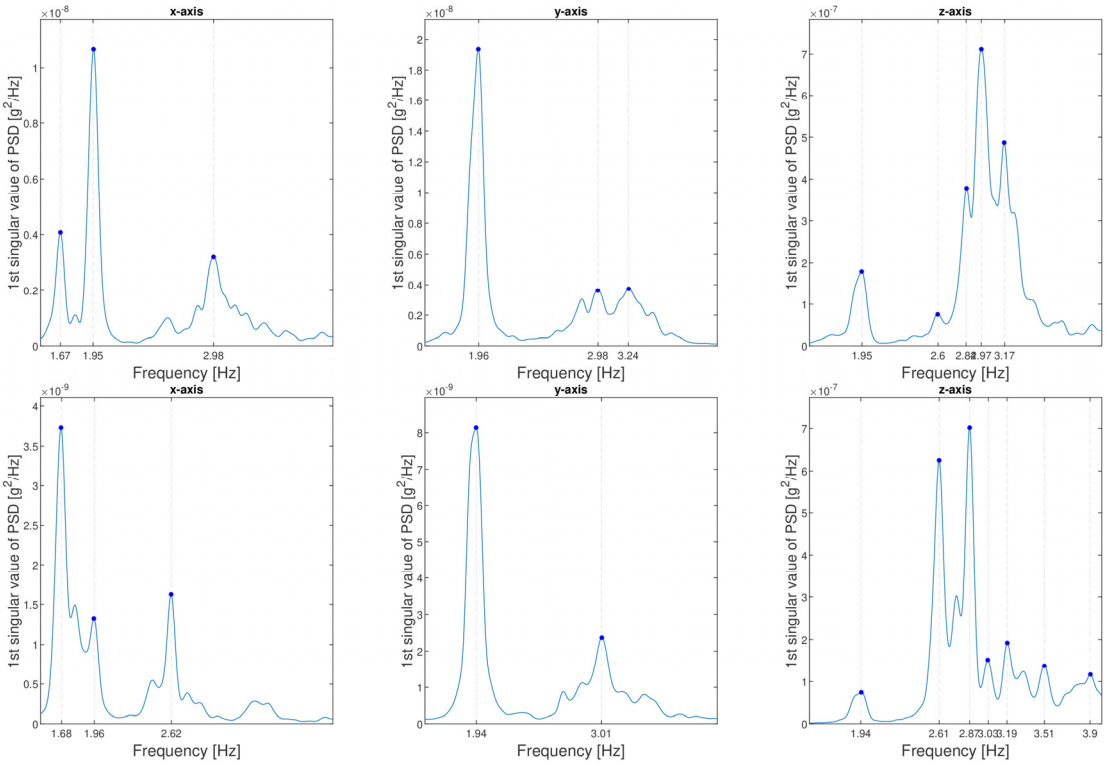

Fig. 23 First singular value of the cross-Power Spectral Density for setup 1 (top) and setup 2 (bottom) with PCB sensors

Table 3 Comparison among numerical and experimental frequencies

Frequencies of the first three dominant mode shapes*, Hz											
x-direction				*y*-direction				*z*-direction			
Mode	FE	Test setup		Mode	FE	Test setup		Mode	FE	Test setup	
		1	2			1	2			1	2
1	1.77	1.67	1.68	4	2.11	1.96	1.94	4	2.11	1.95	1.94
3	1.94	1.95	1.96	8	2.48	-	-	8	2.48	2.6	2.61
25	3.47	2.98	-	14	2.75	2.98	3.01	24	3.42	3.17	3.19

*A cell with a dash indicates data that has not been experimentally detected

use of low-cost, low-power WSNs based on output-only modal analysis of structures (Krishnamurthy *et al*. 2008). In this respect, the low-cost MEMS equipped with GPS used in this experimental campaign is an ideal candidate for deploying a vast network on large structures.

To measure the dynamic response of the canopy two different setups were used with the sensors placed in the position shown in Fig. 22. For each setup, at least 30 minutes of data were recorded in the three axes. Modal shapes and frequencies were retrieved by means of different output-only identification techniques, namely the Stochastic Subspace Identification (SSI) and the Frequency Domain Decomposition (FDD).

The first singular value of the cross-Power Spectral Density (c-PSD) as obtained from the FDD technique is shown in Fig. 23 for setup 1 and 2. The corresponding frequencies and their correlation with the FE numerical results of previous Sections are shown in Table 3.

As expected, the peaks in the *z*-axis are at least one-order of magnitude higher than those in the other directions due to slenderness of the structure. This is mostly relevant for the measurement point at the free end of the canopy as shown in Fig. 24.

Considering the low number of experimental measurement points (which does not allow to compare the mode shapes) and the high modal density shown by the numerical model, the comparison among experimental and numerical results is not straightforward and a practical solution strategy must be selected. Table 3 shows the numerical and experimental frequencies of the first three dominant mode shapes, where numerical dominant modes are the ones corresponding to the maximum values of participating mass (see Figs. 16 and 17). In detail, a quantitative comparison among the numerical and experimental frequencies proves that the FE model is in good agreement with the experimental outcomes, even if the numerical model tends to be more flexible than the real structure (with an average percentage reduction of the 5%).

A comparison of the acceleration PSD registered with the three instruments is shown in Fig. 25 for the

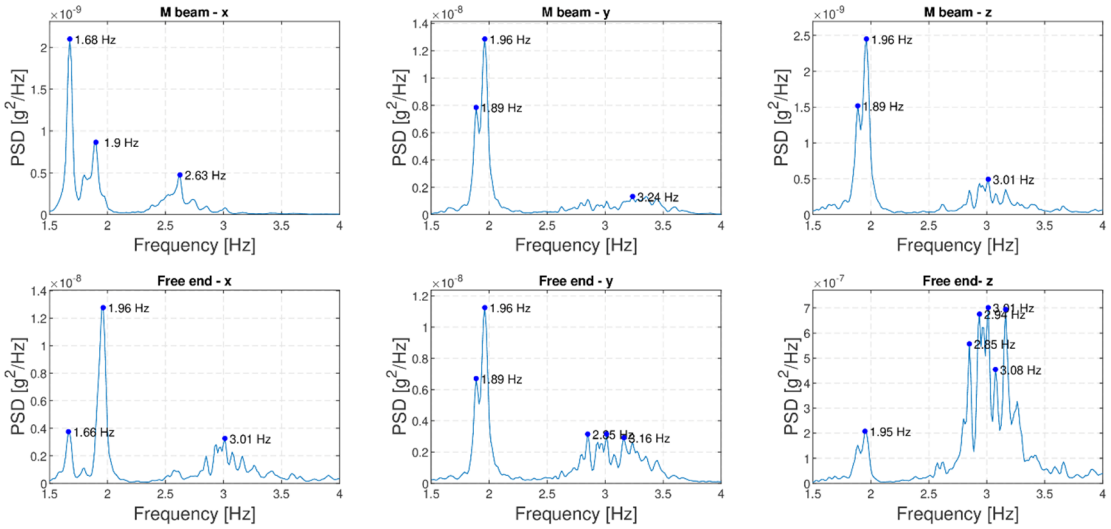

Fig. 24 Power Spectral Density of the signals acquired with the PCB sensors both at the free-end and on the M-beam for setup 1

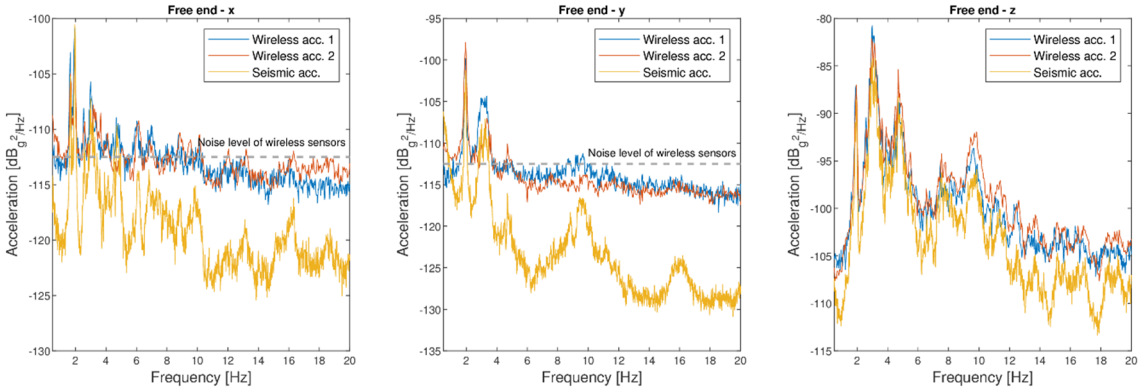

Fig. 25 Acceleration Power Spectral Density of the signals acquired at the free end for setup 1

(a) Young's modulus (b) Density of the ferrocement

Fig. 26 Sensitivity analysis of the FE model vs the tuning parameters

experimental setup 1. The different sensitivities of the sensors are clearly seen in the figure, with the PCB providing the highest accuracy in detecting the peaks in all the three axes. On the contrary, both Tromino and Wisesensing are not able to discriminate peaks at frequencies higher than 6 Hz, since their energy content is below the instrument noise level, which is shown in the figures as grey dashed line and can be estimated to be around 110-115 dB.

This preliminary analysis served us to identify the mode shapes than can be detected and monitored with a SHM wireless sensor network. As Fig. 25 shows there is always a trade-off between the number of detectable modes, i.e., the sensor accuracy, and its cost and easiness of positioning. It is opinion of the authors that a SHM system must privilege robustness over accuracy and, in this sense, having a larger number of sensors to track changes in fewer modes is the approach to follow.

4.2 Model calibration

With the intent of calibrating the numerical model with

the experimental outcomes shown in the previous paragraph, a model calibration is performed. Since visual inspection did not suggest any structural damages, this calibration is suitably carried out considering as tuning parameter the Young's modulus and the unit weight of ferrocement, whose relevant values are surely affected by more uncertainties than the corresponding values indicated in Table 1 for concrete and steel. The result of the sensitivity analysis of the model, when the two tuning parameters are individually altered, is in Fig. 26, where only the frequencies of the dominant modes considered in Table 3 are conveniently shown.

Since the numerical model was stiffer than the real structure, in order to have a better match among the data, it is necessary to calibrate the model by reducing the stiffness (the Young's modulus) of the ferrocement (initial value of 30.6 GPa) and/or by increasing its density (initial value of 20 kN/m^3). However, starting from the physical meaning of these tuning parameters, the two values of 26 GPa and 24 kN/m^3 are here imposed as lower and upper thresholds for the Young's modulus and the density, respectively. Assuming as error function the following (here '$f_{,num}$' and '$f_{,exp}$' stand for numerical and experimental frequencies, respectively, whereas the subscripts i, j and k refer to the i-th mode shape, j-th setup and k-th direction)

$$RMSE = \sqrt{\frac{1}{18}\sum_{k=x,y,z}\left(\sum_{j=1,2}\left(\sum_{i=a,b,c}\left(\frac{f_{exp,ijk}-f_{num,ijk}}{f_{num,i}}\right)^2\right)\right)}$$

where $a,b,c = \{1,3,25 \text{ for } k=x \quad 4,8,14 \text{ for } k=y \quad 4,8,24 \text{ for } k=z\}$

that is, the Root-Mean-Square Error evaluated on the dominant normalized frequencies, the initial solution has an $RMSE$ of 0.076, while the final (optimized) one of 0.063, i.e., a value almost one fifth smaller of the initial. This calibrated numerical model is the one obtained by considering the Young's modulus and the density of the ferrocement equal to the relevant thresholds.

This initial model calibration has been carried out comparing only the experimental and numerical frequencies. Indeed, the limited number of measurement points used in preliminary experiments did not provide reliable information on the mode shapes. In the sensor network proposed in Section 5.1, a larger number of sensors will be adopted and this will allow a more accurate assessment of the mode shapes to be used in the model updating algorithm.

The dominant frequencies of both initial and final models are in Fig. 27, together with the relevant experimental values, intended as the average frequency of all setups and directions, when several data are available for the same mode shape. As clearly shown by the plot, the final model still tends to be more flexible than the real structure, but the average percentage reduction among experimental and numerical frequencies is now very low, equal to 2% (5% for the initial model). Further analyses (laboratory tests on ferrocement samples) are scheduled to check the stiffness and the density here identified by the model calibration.

5. A low-cost proposal of sensors network for structural health monitoring

5.1 Monitoring system design

From the perspective of SHM, static and dynamic measurements are complementary. On the one hand, static monitoring allows the identification of the occurrence of structural damages associated with degradation phenomena, such as corrosion and crack opening, by measuring physical quantities (e.g., displacements and inclinations) in characteristic sections and repeating the measure over time at regular intervals. On the other hand, dynamic monitoring aims to analyze the evolution of structural behavior over time and to point out the onset of high levels of vibration, which is a real time investigation on potential situations of immediate danger. At the same time, changes in vibration signals are the dynamic counterpart of any progressive phenomenon of structural damage revealed through static approaches.

According to the previous results, showing the possibility of adopting the canopy for a suitable dynamic characterization of the whole stadium, the experimental setup proposed for the SHM of Flaminio is mainly intended to acquire the static and dynamic response of the canopy. However, even some critical sections of the underlying reinforced concrete frames are monitored. In detail, the

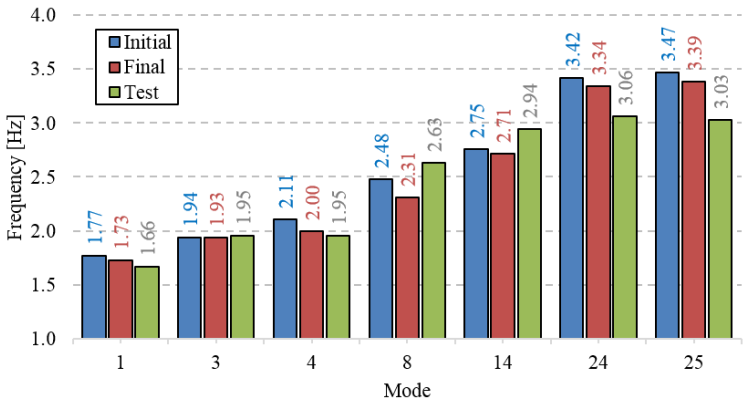

Fig. 27 Comparison among experimental and numerical dominant frequencies

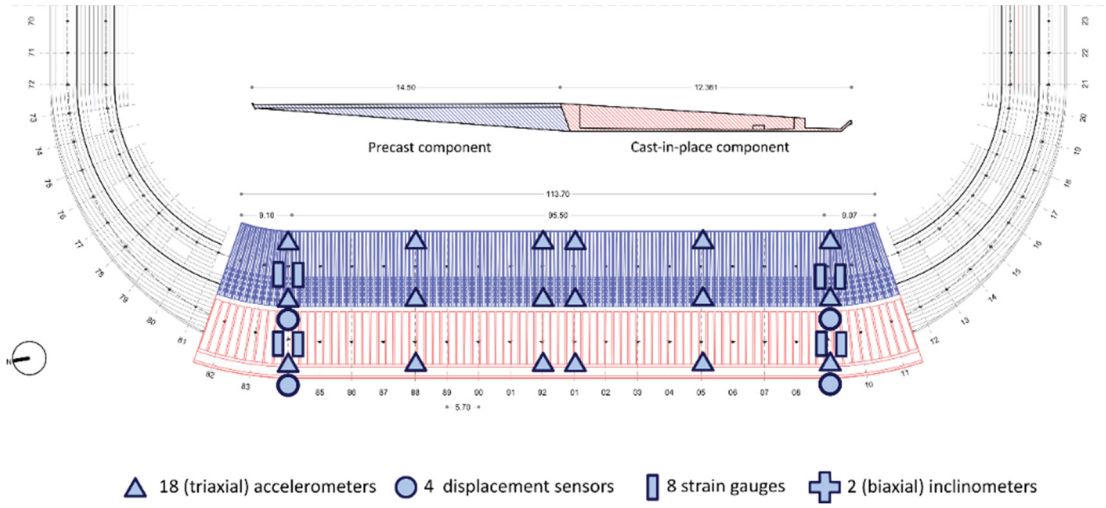

Fig. 28 Sensors placement: plan view of half of the stadium (dimensions are in meters)

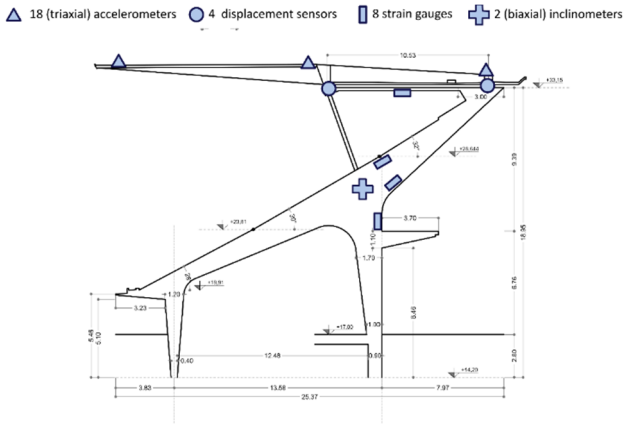

Fig. 29 Sensors placement: elevation view of one frame of the stadium (dimensions are in meters)

network is here designed positioning four kind of sensors along the cited structural elements:

- 18 (triaxial) accelerometers;
- 2 (biaxial) inclinometers;
- 4 position (displacement) sensors;
- 8 strain gauges;

see Fig. 28, for a plan view, and Fig. 29, for an elevation view. This sensor arrangement was guided by the numerical model outcomes and resistance check results (the latter not shown for sake of brevity): three strain gauges and one biaxial inclinometer around the most stressed joint, for each reinforced concrete frames close to the curves of the stadium, where cracks were already noted in the past; two further strain gauges placed in correspondence of the same frames, astride the reinforced concrete ties; eighteen accelerometers arranged on the perimeters of the two portions of the roof and along the two centerlines between the long sides; four displacement sensors around the connections between the roof and the canopy supporting system.

All the mentioned devices are endowed with temperature sensor. In particular, this will allow us to monitor the temperature variations between the intrados and the extrados of the roof and, thus, quantify the thermal effects, also considered by Nervi in his design. Further numerical and experimental studies on the adequacy of this first proposal of sensor network are underway, also in order to verify any feasible failure due to sensor malfunctions, see Chang *et al*. (2017), or, in case of wireless sensors, arising from synchronization issues, see Kim *et al*. (2016).

5.2 Measured data interpretation and management

The data provided by the sensor network described above will be processed in order to: (i) detect the frequencies and the mode shapes according to consolidated methodologies, including the removal of undesired environmental effects; (ii) identify possible structural degradation phenomena or damages linked to variations in frequencies and/or mode shapes (in this respect, the numerical sensitivity analysis, Fig. 26, allows to distinguish the onset of phenomena affecting the roof from the ones regarding the substructure) by applying existing and novel techniques, such as the ones proposed by some of the authors in Lofrano *et al*. (2019, 2020); (iii) compare the experimental static measures with suitable alert thresholds.

On-going works are also devoted to developing an integrated system for a proactive approach to through-life care of the Flaminio Stadium structures. Structural monitoring, with the ensuing model updating and, possibly, capacity evolution tracking, is integrated in a unified environment guiding facility managers and decision-makers. The processes and tools characteristic of a building information modeling (BIM) approach applied to architectural heritage (HBIM) (Bruno and Roncella 2019) provide a suitable solution. HBIM enables to: retrace the historical evolution of the structure; connect documentary evidence via digital databases; combine interdisciplinary data and information models; contain guidelines for conservation and maintenance policies. Thus, the HBIM process, differently from traditional design tools, can efficiently epitomize past, present and future of the Flaminio's life (Romeo *et al*. 2019). In detail, the information gathered via SHM can be stored and linked in

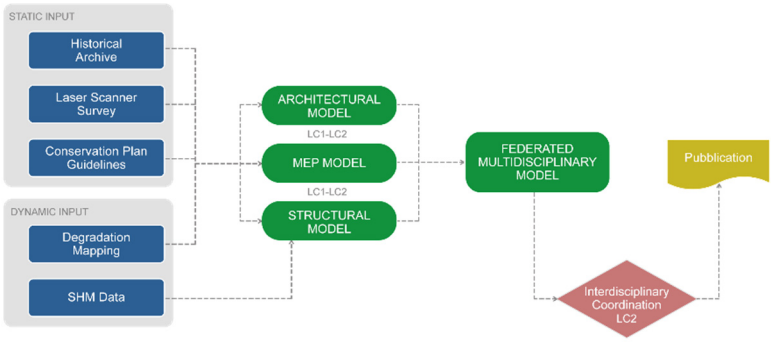

Fig. 30 Dynamic HBIM workflow embedding SHM activities

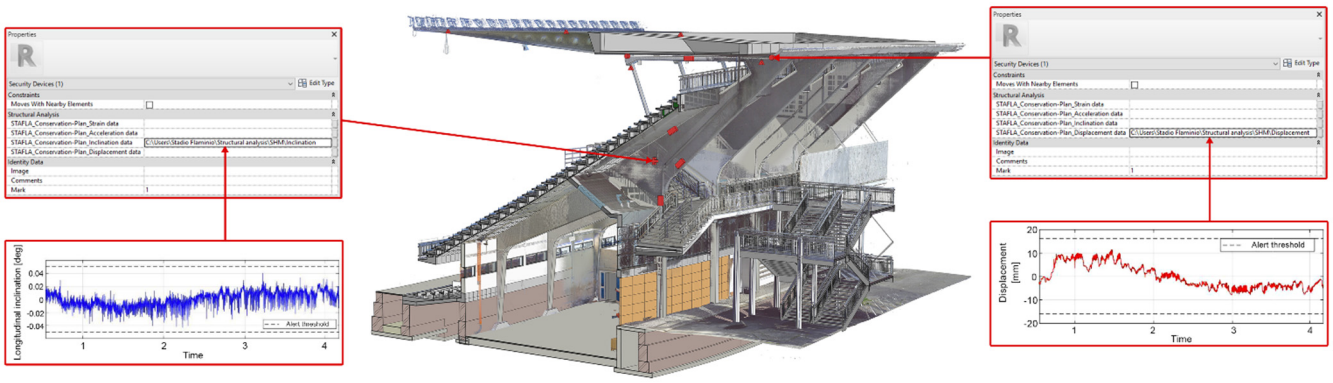

Fig. 31 Point cloud and BIM model overlay of the west grandstand; BIM URL monitoring parameters added to sensors category

a dynamic HBIM model. Irrespective of the type of information, the use of both open data interchange formats (.ifc) and direct interaction formats ease the digital dialogue, through a CDE (Common Data Environment) enabling to share all the produced information.

The proposed process consists of different stages dictated by the HBIM workflow sketched in Fig. 30. The latter can be viewed as a matrix in which four activities intersect with three temporal phases. The activities consist of data input, data segmentation, data structuring and data representation, while the temporal phases consist of the original configuration (past), current condition (present) and conservation plan (future). The core of the outlined methodology is represented by the data structuring phase in which SHM data and their processing are introduced in the HBIM platform; thus, continuous or periodic measurement and analyses of key structural and environmental parameters under operating conditions are made available to users (e.g., Fig. 31), i.e., facility managers, for visualization, sharing and decision-making purposes.

The possibility of handling a large amount of heterogeneous information, makes the HBIM approach comprehensive methodology useful to protect and manage heritage assets.

6. Conclusions

The Flaminio Stadium represents an exemplary use of precast and cast on site reinforced concrete and ferrocement. The numerous Nervi's outstanding design solutions make this stadium a modern monument, firmly rooted in the urban panorama of the "Eternal City". In this work, the structural features of the Flaminio Stadium were presented aiming at highlighting their peculiarities mainly concerning the grandstand load bearing structure and the west grandstand roof.

The adoption of a simplified shell-beam FEs based model of the canopy was justified through a direct comparison with a solid FEs based one. On the contrary, the analysis carried out on the structural frames of the stadium evidenced the need to adopt shell FEs, instead of reduced order models based on equivalent beam FEs.

Dynamic tests were carried out on the canopy, to validate the numerical model, to investigate and quantify the response to environmental loadings and to infer the adequate instrumentation setup enabling to capture the desired structural features. The results, showed in Section 4, highlighted how environmental induced vibrations can or cannot be adequate depending on both the monitored direction and the accelerometer device. The comparison between experimental and numerical results was developed considering the dominant numerical and experimental frequencies. The formers were identified as the ones corresponding to the maximum participating mass percentage, while the experimental counterparts refer to maxima of Fourier transform. The subsequent calibration of the numerical model with the experimental outcomes was carried out by adopting as tuning parameter the Young's modulus and the unit weight of ferrocement. The ferroce-

ment mechanical parameters estimated via model calibration are worth being further investigated via laboratory testing.

A proposal of sensors network for SHM, pivoting on a suitable instrumentation of the canopy, is eventually presented together with a dynamic HBIM platform providing a digital synthesis for the implementation of a proactive through-life conservation strategy with a twofold objective: minimize intervention costs and maximize structure service life.

Acknowledgments

FR acknowledges the financial support of Getty Foundation, grant n° R-ORG-201734730. The Authors are grateful to Roberto Ziantoni and Roberta Sulpizio of the Department for Sports and Youth Policies of Rome Municipality for their assistance during the experimental campaign.

References

Adriaenssens, S. and Billington, D.P. (2013), "Nervi's cantilevering stadium roofs: Discipline of economy leads to inspiration", *J. Int. Assoc. Shell Spatial Struct.*, **54**(176-177), 169-178. https://www.scopus.com/inward/record.uri?eid=2-s2.0-84887469023&partnerID=40&md5=9d7c65b3d81f7198db180f784807f66c

Antonucci, M., Trentin, A. and Trombetti, T. (2014), *Pier Luigi Nervi. Gli stadi per il calcio*, Bologna University Press, Bologna, Italy.

Bathe, K.J. (2006), *Finite Element Procedures*, Klaus-Jurgen Bathe, Watertown, MA, USA.

Bentz, E.C., Vecchio, F.J. and Collins, M.P. (2006), "Simplified modified compression field theory for calculating shear strength of reinforced concrete elements", *ACI Struct. J.*, **103**(4), 614-624. https://doi.org/10.14359/16438

Bruno, N. and Roncella, R. (2019), "HBIM for Conservation: A New Proposal for Information Modeling", *Remote Sensing*, **11**(1751), 24 p. https://doi.org/10.3390/rs11151751

Caprioli, A., Vanali, M. and Cigada, A. (2009), "One year of structural health monitoring of the Meazza Stadium in Milan: Analysis of the collected data", *Proceedings of the Society for Experimental Mechanics Series*, 9 p. https://www.scopus.com/inward/record.uri?eid=2-s2.0-84861561446&partnerID=40&md5=caccb796611d37242372cd517a69057f

Chang, C.-M., Chou, J.-Y., Tan, P. and Wang, L. (2017), "A sensor fault detection strategy for structural health monitoring systems", *Smart Struct. Syst., Int. J.*, **20**(1), 43-52. https://doi.org/10.12989/sss.2017.20.1.043

Ciampi, V. and Carlesimo, L. (1986), "A nonlinear beam element for seismic analysis of structures", *Proceedings of the 8th European Conference on Earthquake Engineering*, 8 p.

Consiglio Superiore dei Lavori Pubblici – Italia (Italian Superior Council of Public Works 2018), Aggiornamento delle Norme Tecniche per le Costruzioni (New Italian Building Code), Decreto Ministeriale del 17 gennaio 2018, Gazzetta Ufficiale Supplemento ordinario n. 8 del 20-2-2018 Serie generale – n. 42. [In Italian]

Di Re, P., Addessi, D. and Paolone, A. (2019), "Mixed beam formulation with cross-section warping for dynamic analysis of thin-walled structures", *Thin-Wall. Struct.*, **141**, 554-575. https://doi.org/10.1016/j.tws.2019.04.014

Diord, S., Magalhães, F., Cunha, Á. and Caetano, E. (2017), "High spatial resolution modal identification of a stadium suspension roof: Assessment of the estimates uncertainty and of modal contributions", *Eng. Struct.*, **135**, 117-135. https://doi.org/10.1016/j.engstruct.2016.12.060

Franceschetti, M. (2015), "Stadio Flaminio Roma - Indagini strutturali (Flaminio Stadium of Rome - Structural investigations)", Technical Report as Court Appointed Expert Witness. [In Italian]

Gattulli, V., Lofrano, E., Paolone, A. and Potenza, F. (2019), "Measured properties of structural damping in railway bridges", *J. Civil Struct. Health Monitor.*, **9**(5), 639-653. https://doi.org/10.1007/s13349-019-00358-3

Gazetas, G. (1991), "Formulas and charts for impedances of surface and embedded foundations", *J. Geotech. Eng.*, **117**(9), 1363-1381. https://doi.org/10.1061/(ASCE)0733-9410(1991)117:9(1363)

G.I.A. L.T.D. (2007), Ristrutturazione dello stadio Flaminio di Roma – Rilievo delle strutture e della consistenza del cls (Restoration of the Flaminio stadium in Rome - Survey of the structures and of the consistency of concretes), Technical Report. [In Italian]

ICOMOS-ISC20C (2017), "Approaches to the Conservation of Twentieth Century Cultural Heritage, Madrid-New Delhi document", *International Committee on Twentieth Century Heritage*, 14 p. http://www.icomos-isc20c.org/pdf/madrid-new-delhi-document-2017.pdf

Katili, I. (1993), "A new discrete Kirchhoff-Mindlin element based on Mindlin-Reissner plate theory and assumed shear strain fields - Part I: An extended DKT element for thick-plate bending analysis", *Int. J. Numer. Methods Eng.*, **36**(11), 1859-1883. https://doi.org/10.1002/nme.1620361106

Kim, R.E., Li, J., Spencer, B.F., Jr., Nagayama, T., Mechitov, K.A. (2016), "Synchronized sensing for wireless monitoring of large structures", *Smart Struct. Syst., Int. J.*, **18**(5), 885-909. https://doi.org/10.12989/sss.2016.18.5.885

Krishnamurthy, V., Fowler, K. and Sazonov, E. (2008), "The effect of time synchronization of wireless sensors on the modal analysis of structures", *Smart Mater. Struct.*, **17**(5), Article No. 055018, 13 p. https://doi.org/10.1088/0964-1726/17/5/055018

Lenticchia, E., Ceravolo, R. and Chiorino, C. (2017), "Damage scenario-driven strategies for the seismic monitoring of XX century spatial structures with application to Pier Luigi Nervi's Turin Exhibition Centre", *Eng. Struct.*, **137**, 256-267. https://doi.org/10.1016/j.engstruct.2017.01.067

Lenticchia, E., Ceravolo, R. and Antonaci, P. (2018), "Sensor placement strategies for the seismic monitoring of complex vaulted structures of the modern architectural heritage", *Shock Vib.*, Article No. 3739690, 14 p. https://doi.org/10.1155/2018/3739690

Lofrano, E., Romeo, F. and Paolone, A. (2019), "A pseudo-modal structural damage index based on orthogonal empirical mode decomposition", *Proceedings of the Institution of Mechanical Engineers, Part C: J. Mech. Eng. Sci.*, **233**(23-24), 7545-7564. https://doi.org/10.1177/0954406219885972

Lofrano, E., Paolone, A. and Ruta, G. (2020), "Dynamic damage identification using complex mode shapes", *Struct. Control Health Monitor.*, **27**(12), e2632. https://doi.org/10.1002/stc.2632

Matthews, S., Bigaj-van Vliet, A., Walraven, J., Mancini, G. and Dieteren, G. (2018), "fib Model Code 2020: Towards a general code for both new and existing concrete structures", *Struct. Concrete*, **19**(4), 969-979. https://doi.org/10.1002/suco.201700198

Midas (2018), MIDAS GEN - Analysis reference manual. https://www.cspfea.net

Midas (2020), MIDAS FEA NX - Analysis reference manual.

https://www.cspfea.net

Nervi, P.L. (1933), "Considerazioni tecniche e costruttive sulle gradinate e pensiline per stadi" (Technical and construction considerations on grandstands and canopies for stadia), Casabella: rivista di architettura e di tecnica, December 1933, 10-13. [In Italian]

Nervi, P.L. and Nervi, A. (1960), "Lo Stadio Flaminio a Roma" (The Flaminio Stadium in Rome), Vitrum, 121. [In Italian]

Olmo, C. and Chiorino, C. (2010), Pier Luigi Nervi. Architecture as Challenge, Silvana Editoriale, Milano, Italy

Presidente del Consiglio dei Ministri – Italia (Italian President of the Council of Ministers 2011), Valutazione e riduzione del rischio sismico del patrimonio culturale con riferimento alle Norme tecniche per le costruzioni di cui al Decreto Ministeriale 14 gennaio 2008 (Evaluation and reduction of the seismic risk of cultural heritage with reference to the buildings technical code of January 14th 2008), Direttiva del 9 febbraio 2011, Gazzetta Ufficiale Supplemento ordinario n. 54 del 26-2-2011 Serie generale – n. 47. [In Italian]

Ragusa, S., Rebecchini, S., Napoli, P. and Giorgetti, R. (1959), Lavori di costruzione dello stadio "Flaminio" in Roma (Construction work for the "Flaminio" stadium of Rome), Certificato di collaudo. [In Italian]

Risorse Per Roma S.P.A. (2013), Stadio Flaminio - Stato di conservazione delle strutture (Flaminio Stadium - State of preservation of the structures), Technical Report. [In Italian]

Romeo, F. (2013), "Presenting Nervi's work through scale models: the NerViLaB", *J*. *Int*. *Assoc*. *Shell Spatial Struct*., **54**(176-177), 211-222. https://www.scopus.com/inward/record.uri?eid=2-s2.0-84887451610&partnerID=40&md5=1a66140e59dc4b2933986b2241d4b2f3

Romeo, F. and Di Re, P. (2019), "Structural analysis and safety seismic assessment of the Flaminio Stadium", Technical Report of the Research Project "Keeping it modern".

Romeo, F., Giodice, M., Simione, M. and Ranghiasci, L. (2019), HBIM per il Piano di Conservazione dello Stadio Flaminio di Roma (HBIM for the Conservation Plan of the Flaminio Stadium in Rome), BIM&DIGITAL Awards 19, first prize in Heritage improvement and restoration.

Rossi, S. (2013), "From the ephemeral city to the 'Italy Regions Park' Rome and the regional exhibition of Expo 1911", *Città e Storia*, **8**(1), 9-105. https://www.scopus.com/inward/record.uri?eid=2-s2.0-84915767553&partnerID=40&md5=4b83763f911267626abbdea0d2c6586d

Spacone, E., Ciampi, V. and Filippou, F.C. (1996), "Mixed formulation of nonlinear beam finite element", *Comput*. *Struct*., **58**(1), 71-83. https://doi.org/10.1016/0045-7949(95)00103-N

Sun, Z., Krishnan, S., Hackmann, G., Yan, G., Dyke, S.J., Lu, C. and Irfanoglu, A. (2015), "Damage detection on a full-scale highway sign structure with a distributed wireless sensor network", *Smart Struct*. *Syst*., *Int*. *J*., **16**(1), 223-242. https://doi.org/10.12989/sss.2015.16.1.223

Taerwe, L. and Matthys, S. (2013), *fib model code for concrete structures 2010*, Ernst & Sohn, Wiley, Berlin, Germany.

Tiberi, M., Carbonara, E. and Sforzini, V. (2017), "Sustainable requalification in restricted area: the case study of Flaminio stadium in Rome", *Energy Procedia*, **126**, 305-312. https://doi.org/10.1016/j.egypro.2017.08.234

Viggiani, C. (1993), Fondazioni, Cooperativa Universitaria Editrice Napoletana, Napoli, Italy. [In Italian]

Zhang, L., Wang, T. and Tamura, Y. (2010), "A Frequency–Spatial Domain Decomposition (FSDD) method for operational modal analysis", *Mech*. *Syst*. *Signal Process*., **24**(5), 1227-1239. https://doi.org/10.1016/j.ymssp.2009.10.024.